remote sensing

MDPI

Article

Leveraging Soil Moisture Assimilation in Permafrost Affected Regions

Ankita Pradhan [1], Akhilesh S. Nair [2], J. Indu [1,3,*], Olga Makarieva [4] and Nataliia Nesterova [4]

[1] Department of Civil Engineering, Indian Institute of Technology Bombay, Mumbai 400076, India
[2] Geophysical Institute, University of Bergen and Bjerknes Center for Climate Research, 5007 Bergen, Norway
[3] Interdisciplinary Center for Climate Studies, Indian Institute of Technology Bombay, Mumbai 400076, India
[4] Institute of Earth Sciences, Saint Petersburg State University, 199034 St. Petersburg, Russia
* Correspondence: indusj@civil.iitb.ac.in

Abstract: The transfer of water and energy fluxes between the ground and the atmosphere is influenced by soil moisture (SM), which is an important factor in land surface dynamics. Accurate representation of SM over permafrost-affected regions remains challenging. Leveraging blended SM from microwave satellites, this study examines the potential for satellite SM assimilation to enhance LSM (Land Surface Model) seasonal dynamics. The Ensemble Kalman Filter (EnKF) is used to integrate SM data across the Iya River Basin, Russia. Considering the permafrost, only the summer months (June to August) are utilized for assimilation. Field data from two sites are used to validate the study's findings. Results show that assimilation lowers the dry bias in Noah LSM by up to 6%, which is especially noticeable in the northern regions of the Iya Basin. Comparison with in situ station data demonstrates a considerable improvement in correlation between SM after assimilation (0.94) and before assimilation (0.84). The findings also reveal a significant relationship between SM and surface energy balance.

Keywords: permafrost; soil moisture; precipitation; streamflow; assimilation; Noah LSM

Citation: Pradhan, A.; Nair, A.S.; Indu, J.; Makarieva, O.; Nesterova, N. Leveraging Soil Moisture Assimilation in Permafrost Affected Regions. *Remote Sens.* **2023**, *15*, 1532. https://doi.org/10.3390/rs15061532

Academic Editors: Gabriel Senay and Qiusheng Wu

Received: 29 January 2023
Revised: 26 February 2023
Accepted: 1 March 2023
Published: 10 March 2023

1. Introduction

Permafrost conditions have a strong influence on the regional moisture flow through the vadose zone and groundwater dynamics [1–4]. The development, distribution, and evolution of permafrost are significantly impacted by soil moisture, notably by heat convection and advection along flow trajectories via influencing surface runoff [1,5,6]. This interaction, together with feedback from physical [7–9], chemical [10–12], and biogeochemical processes [13,14], generates complicated permafrost–soil moisture-groundwater dynamics in regions with permafrost. Permafrost controls drainage, routing, storage of water, as well as surface and sub-surface distribution, which has a substantial impact on terrestrial hydrological processes. Furthermore, permafrost conditions prevent the vertical flow of water through the vadose zone [15], which results in flooding conditions, in case of extreme precipitation events [16].

Soil Moisture (SM) estimates are crucial components for regional hydrology, as they convert incoming precipitation to infiltration and runoff [17–21]. SM remains a crucial land surface state estimate which, when used as a forcing variable in a land surface model, is capable of contributing to improved prediction in different fields, such as weather [22], climate studies [23], hydrology [24,25], hazard mitigation of hydrological extreme events [26–29], and water resources management [30–33]. The physics of the model, the quality of the forcing data, the input land surface parameters, and the initialization of the land surface all contribute to the Land Surface Model's (LSM) prediction accuracy of land surface states [34–36]. By coupling the model's prediction with remote sensing measurements, Data Assimilation (DA) provides enormous potential for enhancing LSM predictive powers [37–40].

Prior research has examined the impact of SM assimilation on LSM forecasting [19,21,35,41,42]. The Global Land Data Assimilation System (GLDAS) is a global implementation of the concept of data assimilation on multiple LSMs (GLDAS; [43]). GLDAS offers global land surface data at three-hourly intervals from different LSMs and two distinct spatial resolutions [21]. Data assimilation incorporates complications connected with data processing, computing load for a geographically extensive research area, and inputs from remotely sensed observations for the status of the land surface [44–47]. Previous research has largely concentrated on the effectiveness of SM assimilation in non-permafrost environments. Moreover, there is a lack of detail in global studies on SM DA on the strategy to assimilate satellite SM when soil is covered in snow and moisture is frozen. We address this issue in our study by explicitly carrying out SM assimilation over permafrost-affected areas. Furthermore, we investigate how SM assimilation influences SM dynamics and its impact on streamflow estimates during the next season.

Despite the importance of permafrost to hydrology, our understanding of the processes that influence water flow and storage during permafrost thaw is limited [48–50]. Previous research has attributed changes in hydrological regimes to a thickening active layer and melting permafrost, but few have explored the response of runoff mechanisms and genesis to active layer variation [51,52].

The SM products from different satellite sensors vary in terms of the sensor frequency, the retrieval algorithm used to derive each SM product, and the temporal and spatial resolution [53,54]. The SM assimilation capability may be adversely impacted by the temporal resolution of the observation data [55–57]. Blended SM products can considerably improve the effect of assimilation on SM prediction [58,59]. Despite studies pertaining to the assimilation of SM from a single satellite sensor, the efficiency of assimilating blended SM in permafrost-affected basins is still not well understood. To overcome this, we designed the present study to assimilate blended SM from the European Space Agency (ESA) and check its impact model simulation over a basin subjected to permafrost in Russia.

2. Study Area

The Iya River watershed (Figure 1) belongs to one of Russia's most flood-prone mountainous regions. The extent of seasonally flooded areas in the Irkutsk region reaches 25,000 km^2, about 4% of its total area. A snowmelt-flood often mixes with a rainfall-flood, and in certain years, debris flows exacerbate rainfall floods. Rainfall-flooding in the Iya catchment's southern areas poses the biggest concern. They occur more often, resulting in greater flooded regions and substantial economic damage. In 1984, 1996, and 2001, floods wreaked havoc in the southern section of the Iya watershed, with the July 2001 flood being the most catastrophic [60]. Extreme rainfall-floods devastated the city of Tulun and other villages on the river floodplain in the summer of 2019, on the rivers of the Iya catchment, becoming the most devastating floods in the area [61,62]. The Iya—Tulun stream gauge registered the largest rise in water level during June 2019 (from 474 to 1387 cm over three days), which was the first flood of the year. The Iya River had a second significant flood from 26 July to 4 August 2019, with the maximum water level reaching a mark of 1121 cm. The 1984 flood, which was considered the biggest flood on record until 2019, is similar in size. Numerous variables, including the impacts of climate change, deforestation, logging and fires, and the melting of snow and glaciers, etc., contributed to the June 2019 devastating flood.

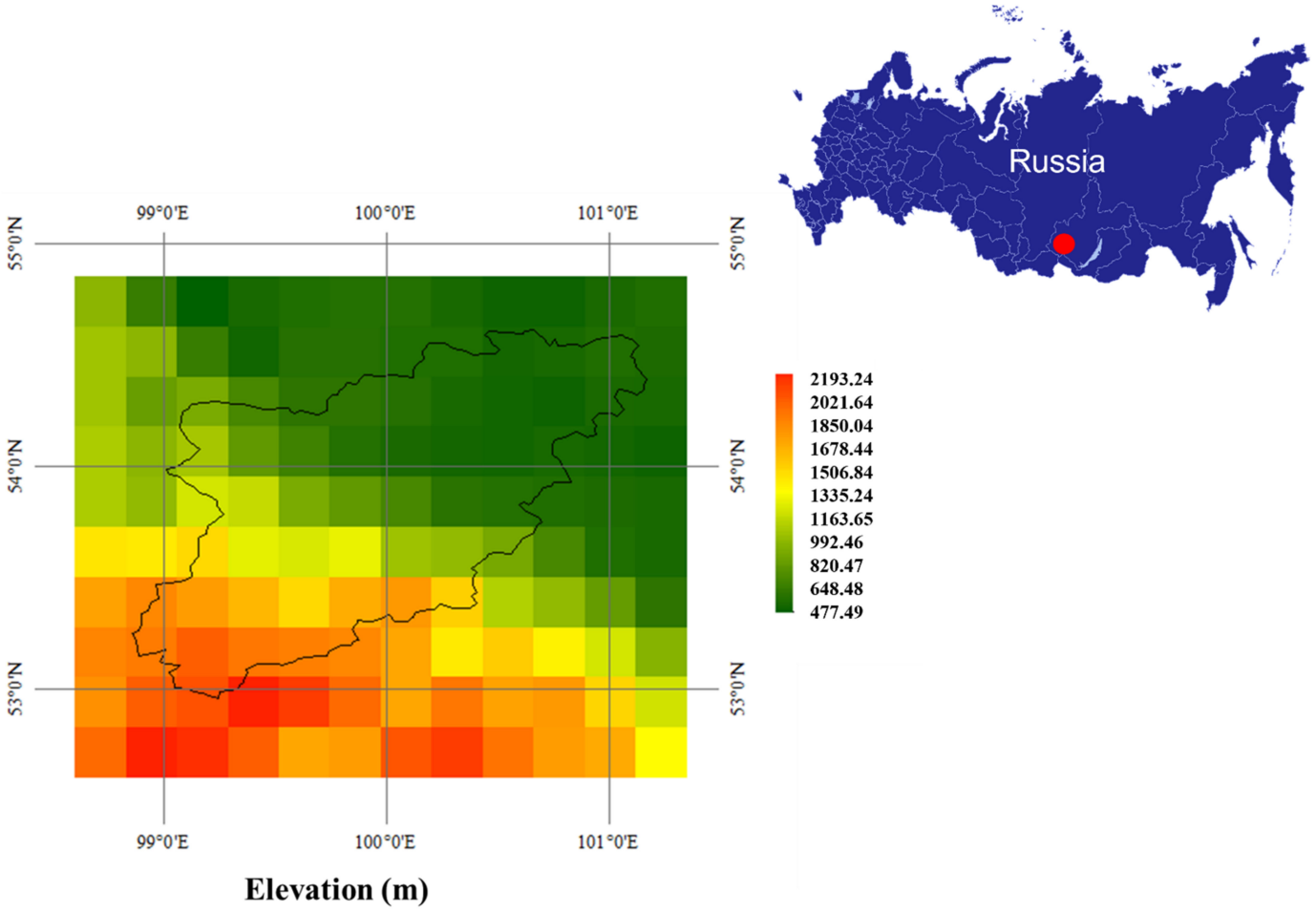

Figure 1. Indicates geographical extent of the Iya River Basin overlaid on SRTM DEM.

3. Model and Data Products

3.1. Noah Land Surface Models

During the 1990s, a comprehensive collaboration of different agencies worked together to improve land surface modeling for the Global Energy and Water Cycle Experiment. The National Center for Atmospheric Research, the National Environmental Satellite Data and Information Service, the U.S. Air Force, NASA, Oregon State University (OSU), and other colleges have engaged in an extensive community effort to create and deploy a standardized Noah LSM. The Noah land surface model is based on the OSU Land Surface Model, which consists of two soil layers with thermal conduction equations for soil temperature and a modified version of Richard's equation for soil moisture [63,64]. The original OSU LSM relied on a plant coefficient to compute the stomatal control of plants to estimate evapotranspiration [63]. Over the years, through continuous community efforts, the latest version of Noah LSM has emerged as a more advanced version of its predecessor. The stand-alone, unified Noah [18–21] used in our study is a medium–complexity model that depends on external meteorological forcing to simulate surface states and surface-to-atmosphere fluxes using physically based equations. The Noah model primarily relies on the conservation of mass and diffusion in Richard's equation to estimate the vertical flow of water in its four-layered soil column. It represents snow as a bulk single layer and represents soil as four layers, with 2 m being the maximum depth. The model assumes downward percolation of water to 2 m depth as the bottom boundary condition of soil moisture.

3.2. Data Products

The stand-alone Noah model needs external forcing for its simulation process. The external forcing mainly consists of near-surface atmospheric parameters, such as temperature, precipitation, wind, pressure and radiation components. Furthermore, the model requires inputs of geostationary parameters defining the soil and vegetation properties.

In this analysis, we use the Global Data Assimilation System meteorological forcing (GDAS). It is a National Centers for Environmental Prediction (NCEP) atmospheric assimilation system [65] that uses a four-dimensional multivariate approach to assimilate in situ and satellite observations into a 3D gridded model space [43]. Four synoptic hours are analyzed for the GDAS operational analysis: 00, 06, 12, and 18 UTC. In addition, each study includes a 3-h and 6-h backdrop forecast. For the present experiment, Noah LSM was used in conjunction with GDAS forcing data updated by the GLDAS team. The specifics of the forcing and geostationary parameters used in this investigation are given in Tables 1 and 2 below.

Table 1. Specification of forcing variables used for Noah LSM.

Variable	Spatial Resolution	Temporal Resolution	Source
Near surface air temperature	0.47° × 0.47°	3 Hourly	GDAS (Source: https://www.ncdc.noaa.gov/dataaccess/model-data/modeldatasets/global-dataassimilation-system-gdas (accessed on 26 April 2021)
Near surface specific humidity			
Total incident shortwave radiation			
Incident Longwave Radiation			
Eastward wind			
Northward wind			
Surface pressure			
Rainfall rate			
Convective rainfall rate			

Table 2. Details of geostationary parameters used in Noah L.SM.

Variable	Spatial Resolution	Source
Landcover	0.01° × 0.01°	Moderate Resolution Imaging Spectroradiometer (MODIS) [https://modis.gsfc.nasa.gov/data/dataprod/mod12.php], (accessed on 26 April 2021)
Soil Texture	0.25° × 0.25°	Food and Agriculture Organization (FAO) [http://www.fao.org/soils-portal/soilsurvey/soil-properties/physical-properties/en/], (accessed on 26 April 2021)
Soil Fraction (clay, sand, silt)	0.25° × 0.25°	FAO [http://www.fao.org/soils-portal/soilsurvey/soil-properties/physical-properties/en/], (accessed on 26 April 2021)
Slope type	0.01° × 0.01°	NCEP_LIS [Source: https://lis.gsfc.nasa.gov/], (accessed on 26 April 2021)
Elevation Data		Shuttle Radar Topographic Mission (SRTM) [http://srtm.csi.cgiar.org/], (accessed on 26 April 2021)
Albedo (Monthly)	0.01° × 0.01°	NCEP_LIS [https://lis.gsfc.nasa.gov/], (accessed on 26 April 2021)
Greenness fraction	0.01° × 0.01°	NCEP_LIS [https://lis.gsfc.nasa.gov/], (accessed on 26 April 2021)

This research employs ESA's CCI V4.2 [66–68] to evaluate the performance of assimilating blended SM products. Various microwave products from active (e.g., ASCAT, SCAT) and passive (e.g., AMSR-E, SMMR, SMAP, SSM/I, SMOS (LPRM), WindSat, Aquarius, TMI) systems are combined to produce them. The combined results are available on the GLDAS Noah climatology with a quarter-degree spatial resolution.

4. Land Data Assimilation Framework and Runoff Routing

The LSM are advanced physics-based numerical models with the ability to predict temporal and spatial variations of land surface state variables. However, these models are subjected to uncertainties from model initialization, parameter, forcing, and physics errors [69–73]. Therefore, through DA, we combine the strengths of hydrologic models as well as observation data to provide a superior surface state estimate. In this study, we particularly evaluate the efficiency of assimilating blended SM products over the Iya Basin in Russia. Our research employs the Land Information System (LIS) [74] architecture established by NASA's Goddard Space Flight Center for absorbing blended SM outputs in Noah LSM. This study is divided into two stages. In the first stage, we implemented a 1-D Ensemble Kalman Filter (EnKF) algorithm [55] to assimilate blended SM in Noah LSM. This research used a thirty-member ensemble because the improvement in outcomes is negligible when the ensemble size exceeds twelve [74]. For further details on the assimilation approach it is recommended to refer to [19,21]. In the second stage of the experiment, runoff estimates from the Noah LSM are routed to the outlet point of catchment to estimate the total river discharge at stations having in situ observations.

4.1. Assimilation Setup for the Iya River Basin in Russia

We assimilate the blended SM from the European Space Agency (ESA) Climate Change Initiative (CCI) in the Noah LSM for a river basin in Russia. The Iya River Basin (Figure 1) is located in southeastern Siberia, between 98.85°E to 101.17°E longitude and 52.94°N to 54.62°N latitude with a total area of 14,500 km^2. It is susceptible to four primary weather conditions: spring (April to May), summer (June to August), fall (September to October), and winter (November to March). This basin is subjected to permafrost, which is one of the major challenges in SM simulation due to its high heterogeneity. In this study, we explore the ability of satellite SM assimilation to improve LSM-simulated seasonal dynamics of the Iya Basin. The details of the methodology flowchart are shown in Figure 2.

The assimilation setup adopted for this study is 1-D Ensemble Kalman Filter (EnKF) for integrating ESA CCI SM into Noah. However, the major challenge in this study region is permafrost. Owing to this, the soil temperature in the basin remains below freezing point during major parts of the year. In such conditions, assimilating satellite SM can lead to uncertainty due to frozen moisture components. Therefore, for this experiment, we only assimilate SM when the temperature is above freezing point (i.e., during the summer season), as shown in Figure 3. Such a simulation setup will also help to evaluate the memory of SM assimilation, as the improvement in other seasons will be only due to improved states during summer.

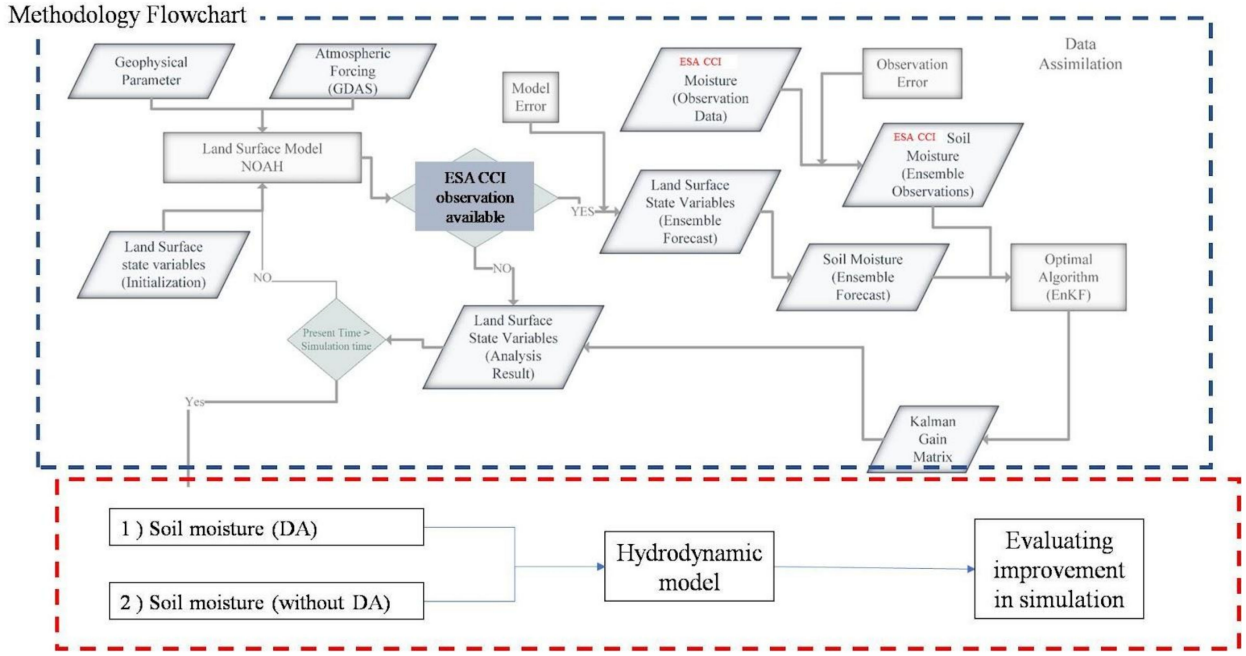

Figure 2. Methodology flowchart showing Stage 1 (Blue box) and Stage 2 (Red box).

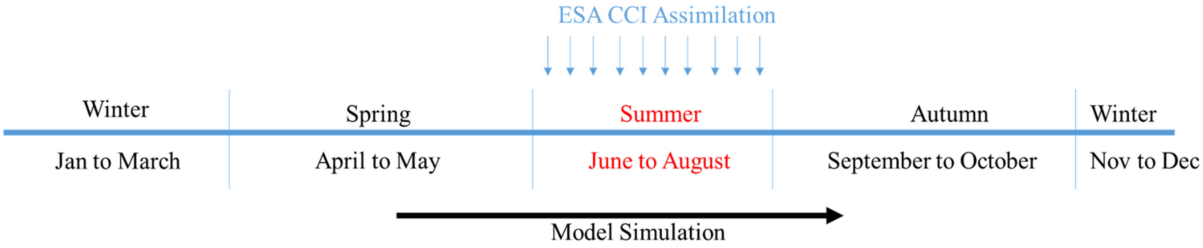

Figure 3. Time frame indicating the assimilation window of ESA CCI SM.

4.2. Routing of Runoff Estimates from LSM

Noah LSM provides runoff estimates for each grid cell. These grid cells from the LSM simulation are routed to the outlet point of the catchment to estimate the total river discharge at stations having in situ observations. The individual grid cells, which are independently modeled, do not have horizontal water flow. Due to the fact that the Noah LSM only models non-uniformly distributed runoff time-series for each cell, a separate model was required to transport cell surface runoff and base flow to the outlet. Research was conducted by [75] to build a horizontal routing model that could be connected to grid-based LSM. This routing concept prohibits water from flowing back into grid cells from channels, because this water will no longer be included in the water budget. A linearized Saint-Venant equation is used to route the discharge at the basin outflow. The fundamental assumption is that runoff from a cell flows in a single direction. In this study, in situ river discharge observations from Tulun and Inga are used to calibrate the routing model. Figure 4 illustrates the routing procedure in its entirety.

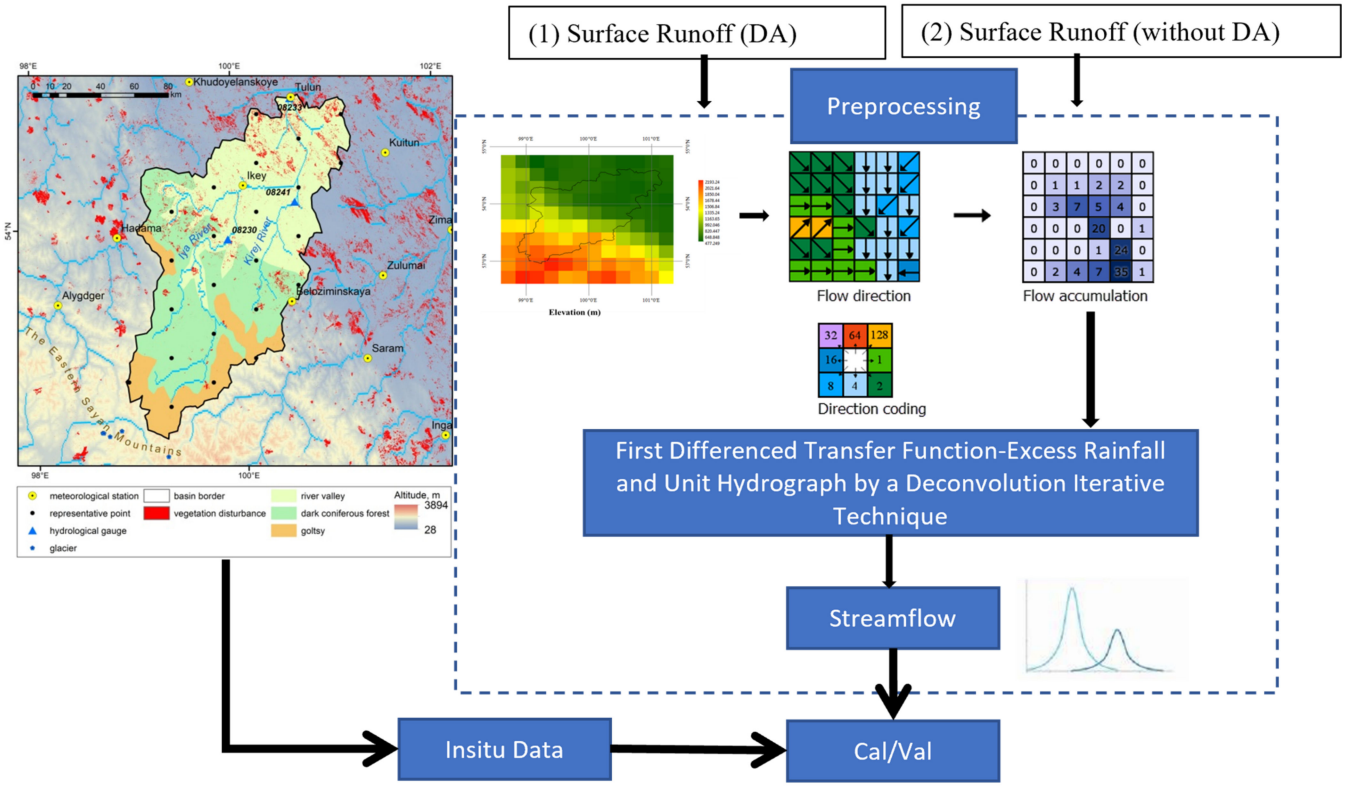

Figure 4. Routing Methodology Flowchart. The grid cells from the LSM simulation are routed to the outlet point of the catchment to estimate the total river discharge at stations having in situ observations. The accumulated flow generates a hydrograph, which is validated with field in situ data.

5. Results

5.1. Enhancement after Assimilating ESA CCI SM

This study demonstrates the improvement in Noah LSM simulations over the permafrost region of Russia [76] (Figure 1) after assimilating the SM product from ESA CCI. As discussed in Section 4.1, SM is only assimilated during the summer season to avoid uncertainty due to frozen moisture. To highlight the improvement, we compare the seasonal mean of SM between open loop and DA. Figure 5 indicates SM during the spring season. It should be noted that no assimilation is performed during the spring season. Therefore, improvement in SM during spring is solely due to improved states during assimilation during the previous summer season. It is noticed that SM decreases after assimilation towards the north of the basin, while SM increases in the southern part of the basin after assimilation.

Figure 6 shows SM during the summer season. During this season, the depth of the active soil layer increases, which is suitable to assimilate SM. From this result, it is observed that, during the summer season, open loop simulation in the northern part of the basin has a dry bias compared to DA run. On the other hand, the southern part of the basin follows a negative trend, where the open loop has a wet bias, which is reduced after assimilation. The assimilated ESA CCI observations have less SM compared to Noah model simulations.

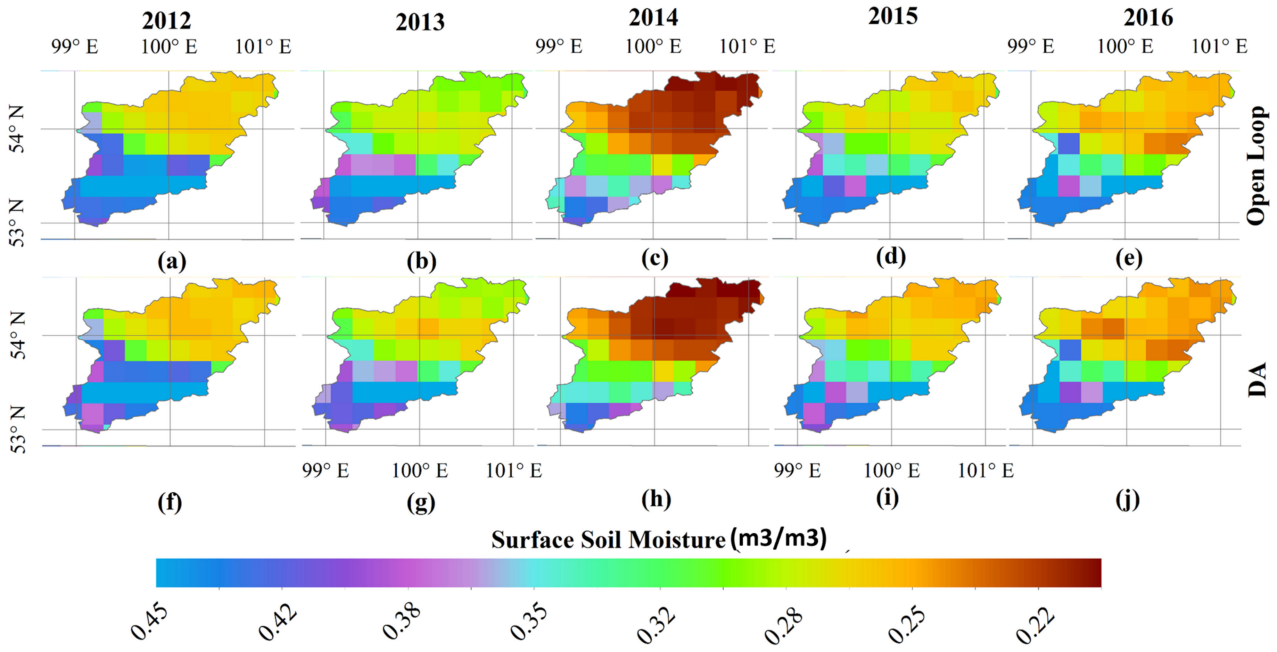

Figure 5. Represents spatial pattern of SM over the Iya Basin during the spring season. Annual mean from open loop are shown in top row (**a**–**e**), from DA in bottom row (**f**–**j**).

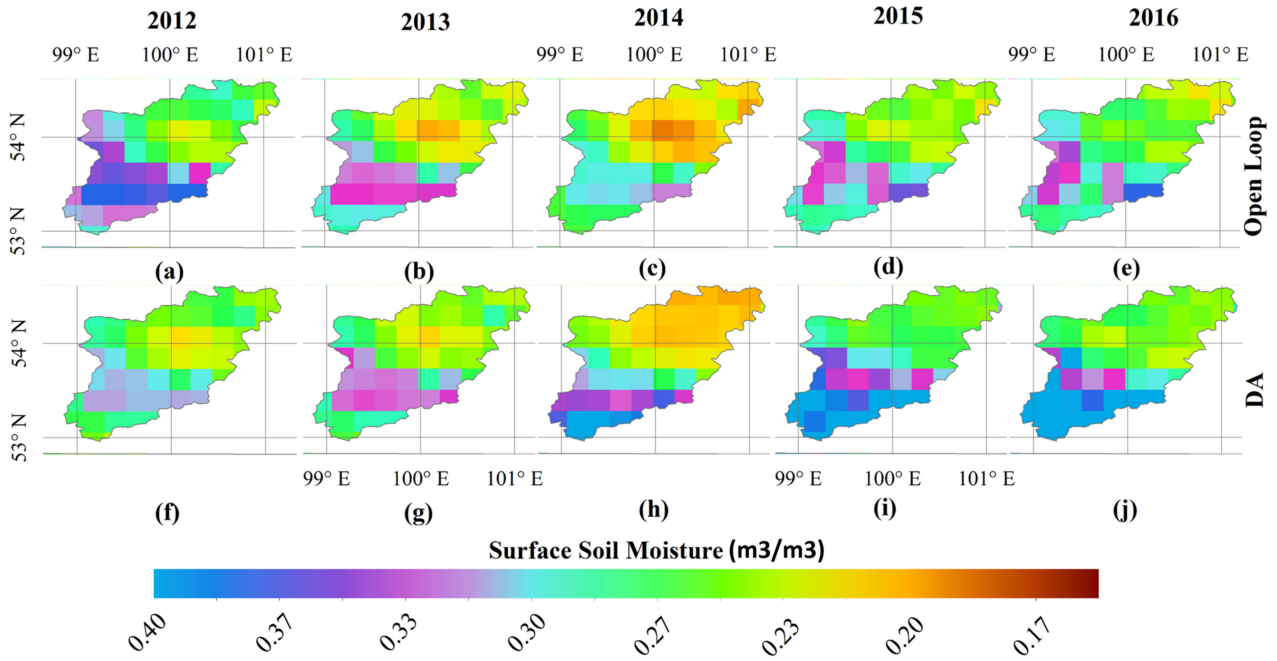

Figure 6. Represents spatial pattern of SM over the Iya Basin during summer season. Annual mean from open loop are shown in top row (**a**–**e**), from DA in bottom row (**f**–**j**).

Similarly, the results are displayed during the autumn season (Figure 7). It should be noted that SM is not directly assimilated during autumn. Therefore, it can be inferred that the improvement in SM is due to the assimilation conducted during the previous season. Results depict a similar behavior, wherein after assimilation, the SM is increased in the northern part of the basin. Similarly, south of the basin exhibits the opposite tendency, with a drop in SM after assimilation due to the EnKF approach's properties; the model results are brought closer to the assimilated observations from ESA CCI.

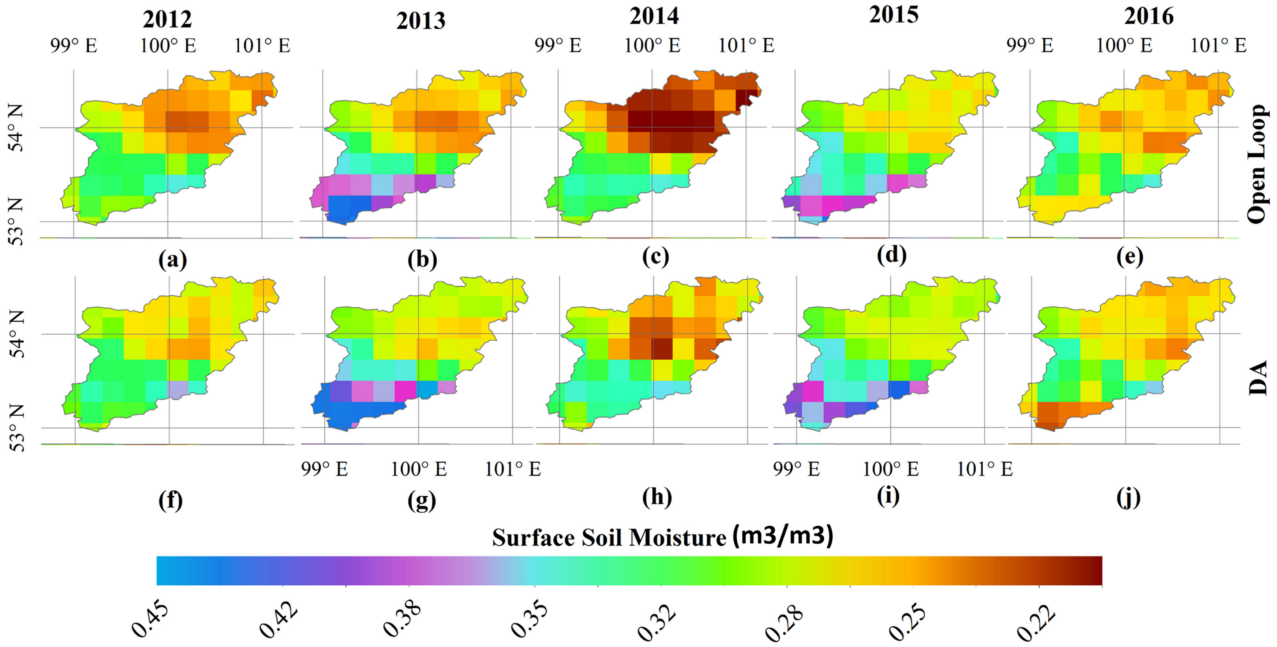

Figure 7. Represents spatial pattern of SM over Iya Basin during autumn season. Annual mean from open loop are shown in top row (**a**–**e**), from DA in bottom row (**f**–**j**).

5.2. Soil Moisture Validation with Independent In-Situ Measurements

The simulated surface soil moisture from open loop and after assimilation are validated with the in situ soil moisture data at two stations: (a) Tulun station and (b) Ikey station (Figure 8). In situ soil moisture is determined by the thermostatic-weight method every ten days in the upper soil layer at a depth of 20 cm.

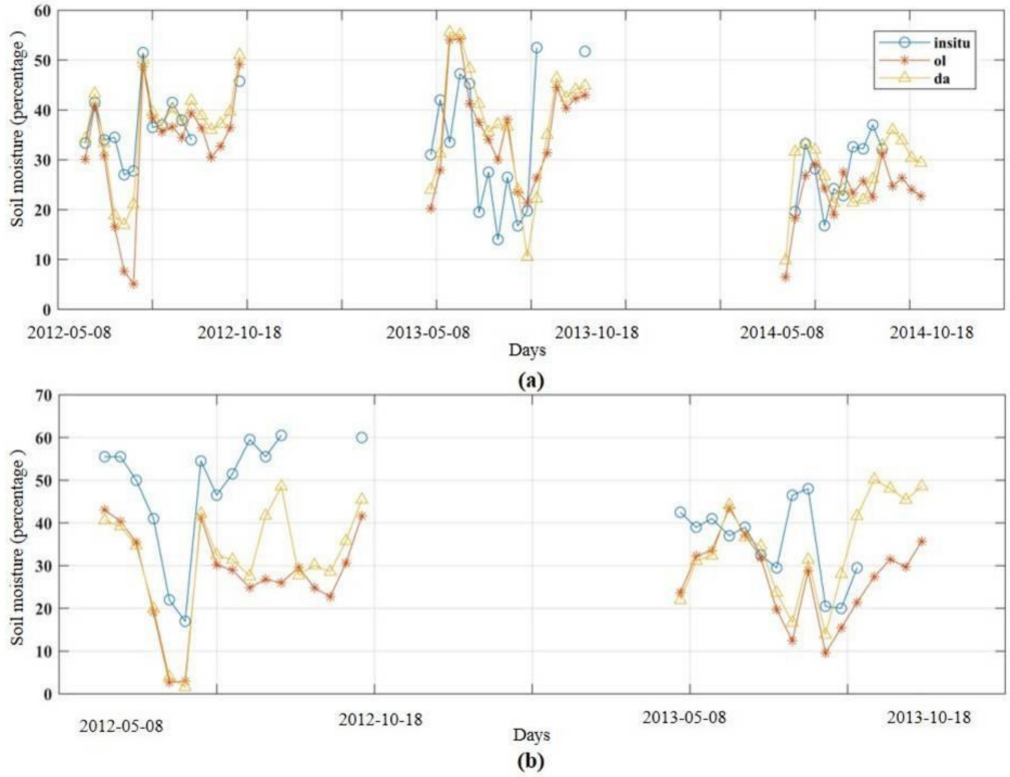

Figure 8. Surface soil moisture validation of open loop and after data assimilation with respect to in situ measurement over (**a**) Tulun station, (**b**) Ikey station.

The simulated assimilated surface soil moisture shows promising results as compared to the open loop results. At the Tulun station, the bias for open loop is 2.2%, whereas after assimilation, the bias is reduced to 0.3%. The correlation coefficient improves from 0.88 in the case of open loop to 0.91 in the case of assimilated soil moisture. At the Ikey station, the bias for open loop is 15.5%, whereas after assimilation, the bias is reduced to 11.5% (Table 3). Furthermore, the correlation coefficient improves from 0.84 in the case of open loop to 0.94 in the case of assimilated soil moisture.

Table 3. Validation of open loop (OL) and after assimilation (PA) with respect to in situ measurement.

Index\Station	Tulun		Ikey	
	PA	OL	PA	OL
Bias	0.3%	2.2%	11.5%	15.5%
Correlation	0.91	0.88	0.94	0.84

5.3. Impact of Assimilation on Streamflow Discharge

Figure 9 shows the spatial plots of surface runoff during 2012, 2013, 2014, and 2015. The top row shows surface runoff for the open loop runs and the second row depicts surface runoff after assimilation. It is noticed that the surface runoff towards the north of basin increases after assimilation. While in the southern part of basin, after assimilation, it moreover remains the same. This is owing to the goltsy rock terrain in the south part, which is less impacted by SM assimilation and, subsequently, runoff. Goltsy rock terrain is a type of bald mountain summit of certain areas in Siberia, Russia. They are barren, rocky, or stony, and only rarely may lichens or stunted small scrubs, such as Siberian pine, grow on them.

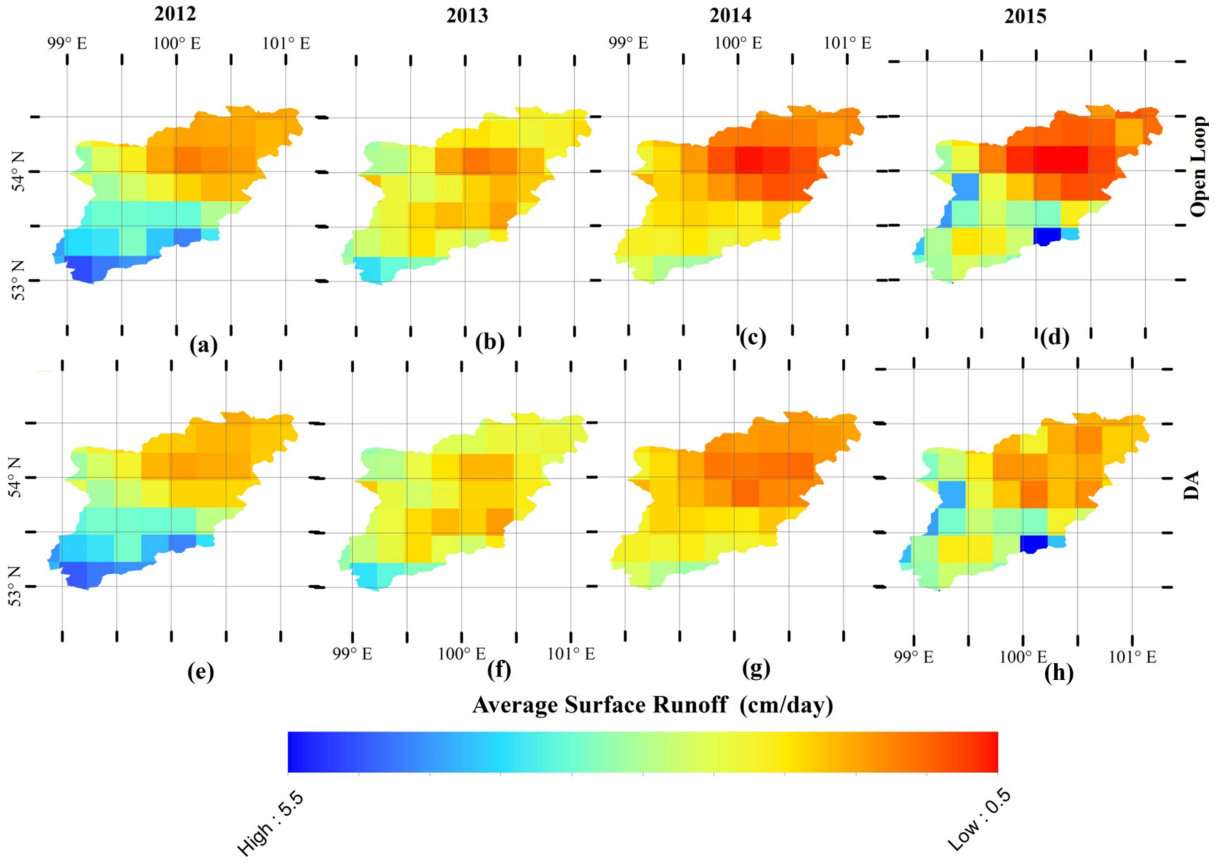

Figure 9. Represents spatial pattern of surface runoff over Iya Basin. Annual mean from open loop are shown in top row (**a**–**d**), from DA in bottom row (**e**–**h**).

These results are consistent with the results of the soil moisture data shown in Figures 5–7.

Figure 10 shows the spatial plots of sub-surface runoff during 2012, 2013, 2014, and 2015. The top row shows the surface runoff for the open loop condition and the second row shows the sub-surface runoff from the assimilated data. Similar to Figure 9, this figure also shows similar results. It is noticed that the surface runoff towards the north of basin increases after assimilation. While in the southern part of basin after assimilation, it moreover remains the same because of the goltsy landform in the south as discussed above. However, there are drastic changes in the years 2014 and 2015.

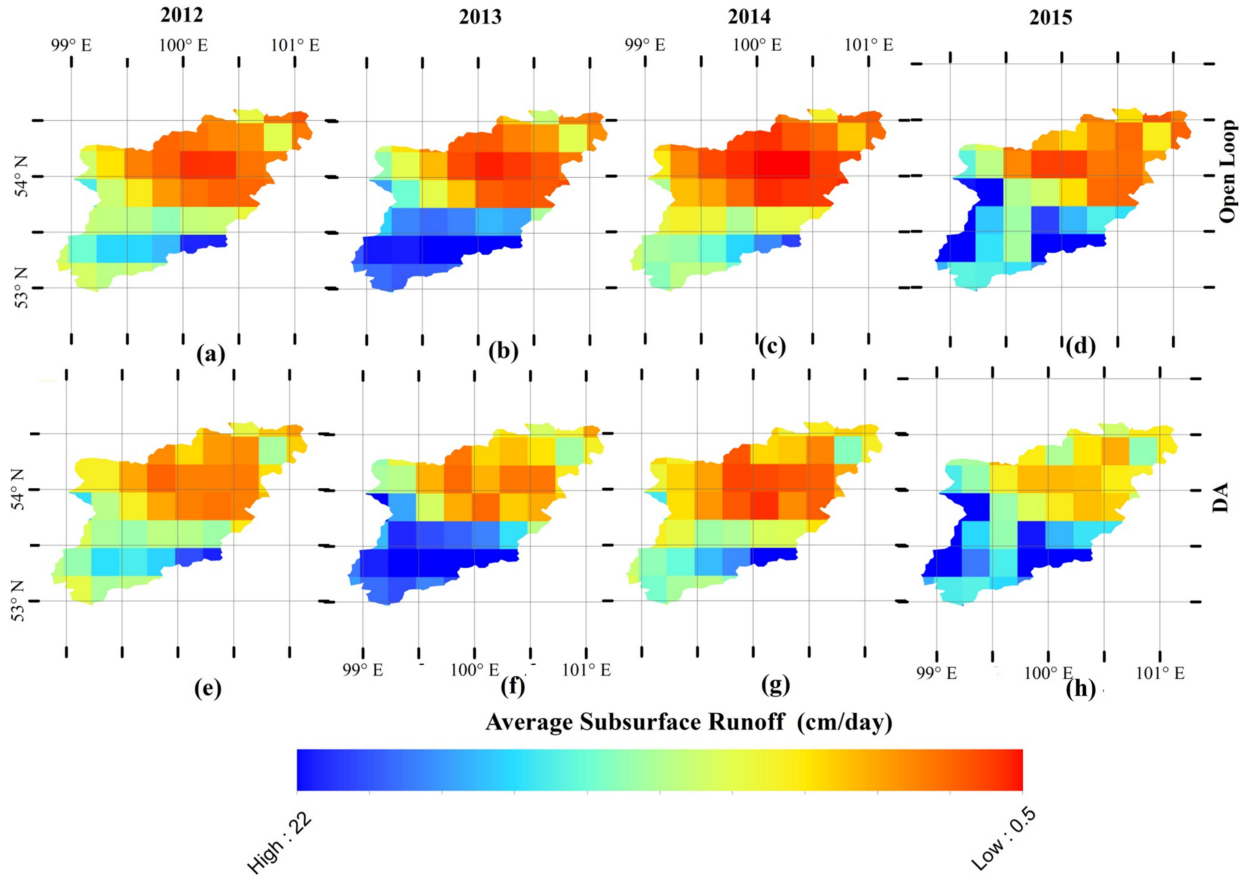

Figure 10. Represents spatial pattern of sub-surface runoff over Iya Basin. Annual mean from open loop are shown in top row (**a**–**d**), from DA in bottom row (**e**–**h**).

Figure 11 represents the time-series of the streamflow generated from routing the surface and sub-surface runoff with respect to the gauge data over the Tulun gauge station. The gray line represents the in situ gauge streamflow. The streamflow generated from the open loop data is represented in orange color, whereas the streamflow generated from the assimilated soil moisture data is shown in blue color. The time-series represented is from the year 2010 to 2015. From the time-series, it is clearly visible that bias in streamflow is more in the case of open loop compared to the assimilated data. The time-series shows that the streamflow generated from assimilated data is closer to the in situ streamflow rather than the streamflow generated from the open loop data. Thereby, it is clear that the improvement in the soil moisture estimates through data assimilation enhances or improves the streamflow predictions in the permafrost-affected regions.

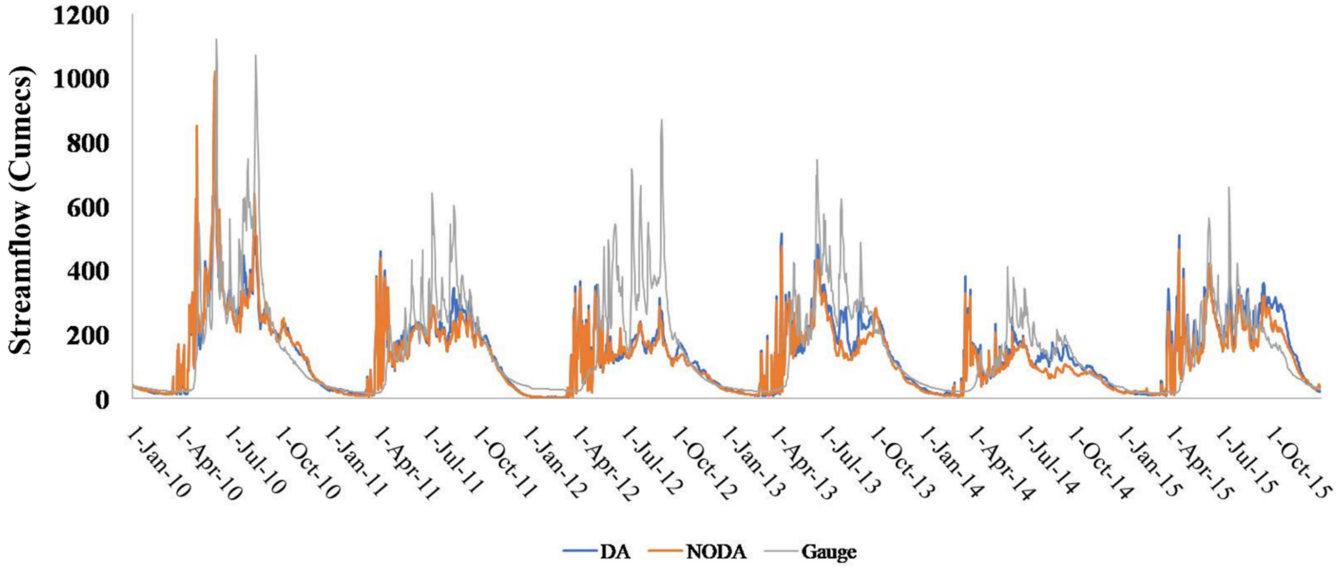

Figure 11. Time-series of streamflow with respect to gauge data over Tulun.

6. Conclusions

The blended SM from the European Space Agency's Climate Change Initiative (ESA CCI) was assimilated over a permafrost basin in Russia. This experiment helps to understand the improvement in Noah model simulation after assimilating blended SM in the permafrost region. The major constraints of permafrost reduced the assimilation window to only the summer season (June, July, August) in this experiment. Therefore, through this study, we demonstrated the impact of assimilating SM in one season and its impact on subsequent seasons. Further analysis on the impacts of DA on permafrost regions warrants attention. This study highlights the efficiency of DA in improving Noah model simulations using blended SM.

Using 1-D Ensemble Kalman Filter (EnKF), this work proposes an effective assimilation configuration for integrating ESA CCI SM into Noah LSM across permafrost-impacted regions. This configuration aids in overcoming the primary obstacles of SM incorporation in permafrost locations. Therefore, the soil temperatures in these places stay below the freezing point for the majority of the year, resulting in permafrost. Due to the frozen moisture component, absorbing satellite SM under such circumstances might lead to ambiguity. Therefore, we only executed SM assimilation in this experiment when the temperature was above freezing (i.e., during the summer season). Such a simulated scenario will also aid in evaluating the memory of SM assimilation, because improvements in future seasons will be solely attributable to summer state improvements. Our study's findings demonstrate the capability of this assimilation setup to enhance SM and, therefore, its influence on streamflow models. The approach used in this study can be applied to any study region where soil moisture data are available. There were no specific region-based limitations used in the study.

Author Contributions: Conceptualization, A.P., A.S.N. and J.I.; formal analysis, A.P.; data curation for soil moisture station observations, O.M. and N.N.; manuscript draft preparation, A.P.; manuscript review and editing, A.S.N., J.I. and O.M.; supervision, J.I. All authors have read and agreed to the published version of the manuscript.

Funding: The study was carried out with the support of RFBR (19-55-80028) and St. Petersburg State University (project 75295876).

Data Availability Statement: All data is available by the request to corresponding author.

Acknowledgments: The authors acknowledge the support from DST supported BRICS Project DST/IMRCD/BRICS/PilotCall3/CCAFRITPOA/2019.

Conflicts of Interest: The authors declare no conflict of interest. The funders had no role in the design of the study; in the collection, analyses, or interpretation of data; in the writing of the manuscript, or in the decision to publish the results.

References

1. Jin, H.; Huang, Y.; Bense, V.F.; Ma, Q.; Marchenko, S.S.; Shepelev, V.V.; Hu, Y.; Liang, S.; Spektor, V.V.; Jin, X.; et al. Permafrost Degradation and Its Hydrogeological Impacts. *Water* **2022**, *14*, 372. [CrossRef]
2. Ramage, J.; Jungsberg, L.; Wang, S.; Westermann, S.; Lantuit, H.; Heleniak, T. Population living on permafrost in the Arctic. *Popul. Environ.* **2021**, *43*, 22–38. [CrossRef]
3. Ran, Y.; Li, X.; Cheng, G.; Nan, Z.; Che, J.; Sheng, Y.; Wu, Q.; Jin, H.; Luo, D.; Tang, Z.; et al. Mapping the permafrost stability on the Tibetan Plateau for 2005–2015. *Sci. China Earth Sci.* **2020**, *64*, 62–79. [CrossRef]
4. Gruber, S. Derivation and analysis of a high-resolution estimate of global permafrost zonation. *Cryosphere* **2012**, *6*, 221–233. [CrossRef]
5. Arenson, L.U.; Harrington, J.S.; Koenig, C.E.; Wainstein, P. Mountain Permafrost Hydrology—A Practical Review Following Studies from the Andes. *Geosciences* **2022**, *12*, 48. [CrossRef]
6. Newman, B.D.; Throckmorton, H.M.; Graham, D.E.; Gu, B.; Hubbard, S.S.; Liang, L.; Wu, Y.; Heikoop, J.M.; Herndon, E.M.; Phelps, T.J.; et al. Microtopographic and depth controls on active layer chemistry in Arctic polygonal ground. *Geophys. Res. Lett.* **2015**, *42*, 1808–1817. [CrossRef]
7. Lara, M.J.; McGuire, A.D.; Euskirchen, E.S.; Tweedie, C.E.; Hinkel, K.M.; Skurikhin, A.N.; Romanovsky, V.E.; Grosse, G.; Bolton, W.R.; Genet, H. Polygonal tundra geomorphological change in response to warming alters future CO_2 and CH_4 flux on the Barrow Peninsula. *Glob. Change Biol.* **2015**, *21*, 1634–1651. [CrossRef]
8. Grosse, G.; Jones, B.; Arp, C. Thermokarst lakes, drainage, and drained basins. In *Treatise on Geomorphology*; Elsevier: Amsterdam, The Netherlands, 2013; Volume 8, pp. 325–353.
9. Andresen, C.G.; Lara, M.J.; Tweedie, C.E.; Lougheed, V.L. Rising plant-mediated methane emissions from arctic wetlands. *Glob. Change Biol.* **2017**, *23*, 1128–1139. [CrossRef]
10. Oberbauer, S.F.; Tweedie, C.E.; Welker, J.M.; Fahnestock, J.T.; Henry, G.H.; Webber, P.J.; Hollister, R.D.; Walker, M.D.; Kuchy, A.; Elmore, E.; et al. Tundra CO_2 Fluxes in Response to Experimental Warming across Latitudinal and Moisture Gradients. *Ecol. Monogr.* **2007**, *77*, 221–238. [CrossRef]
11. Kanevskiy, M.Z.; Shur, Y.; Jorgenson, T.; Brown, D.R.; Moskalenko, N.G.; Brown, J.; Walker, D.A.; Raynolds, M.K.; Buchhorn, M. Degradation and stabilization of ice wedges: Implications for assessing risk of thermokarst in northern Alaska. *Geomorphology* **2017**, *297*, 20–42. [CrossRef]
12. Liljedahl, A.K.; Boike, J.; Daanen, R.; Fedorov, A.N.; Frost, G.V.; Grosse, G.; Hinzman, L.D.; Iijma, Y.; Jorgenson, J.C.; Matveyeva, N.; et al. Pan-Arctic ice-wedge degradation in warming permafrost and its influence on tundra hydrology. *Nat. Geosci.* **2016**, *9*, 312–318. [CrossRef]
13. Throckmorton, H.M.; Heikoop, J.M.; Newman, B.D.; Altmann, G.L.; Conrad, M.; Muss, J.D.; Perkins, G.B.; Smith, L.J.; Torn, M.S.; Wullschleger, S.D.; et al. Pathways and transformations of dissolved methane and dissolved inorganic carbon in Arctic tundra watersheds: Evidence from analysis of stable isotopes. *Glob. Biogeochem. Cycles* **2014**, *29*, 1893–1910. [CrossRef]
14. Frey, K.E.; McClelland, J.W. Impacts of permafrost degradation on arctic river biogeochemistry. *Hydrol. Process.* **2009**, *23*, 169–182. [CrossRef]
15. Walvoord, M.A.; Kurylyk, B.L. Hydrologic Impacts of Thawing Permafrost—A Review. *Vadose Zone J.* **2016**, *15*. [CrossRef]
16. Jafarov, E.E.; Coon, E.T.; Harp, D.R.; Wilson, C.J.; Painter, S.L.; Atchley, A.L.; Romanovsky, V.E. Modeling the role of preferential snow accumulation in through talik development and hillslope groundwater flow in a transitional permafrost landscape. *Environ. Res. Lett.* **2018**, *13*, 105006. [CrossRef]
17. Nair, A.S.; Mangla, R.; Thiruvengadam, P.; Indu, J. Remote sensing data assimilation. *Hydrol. Sci. J.* **2022**, *67*, 2457–2489. [CrossRef]
18. Krishnan, S.; Nair, A.S.; Indu, J. Simulation of Passive Microwave Data toward Efficient Assimilation over Indian Subcontinent. *IEEE Geosci. Remote Sens. Lett.* **2021**, *18*, 851–855. [CrossRef]
19. Nair, A.S.; Indu, J. Improvement of land surface model simulations over India via data assimilation of satellite-based soil moisture products. *J. Hydrol.* **2019**, *573*, 406–421. [CrossRef]
20. Shrestha, A.; Nair, A.S.; Indu, J. Role of precipitation forcing on the uncertainty of land surface model simulated soil moisture estimates. *J. Hydrol.* **2020**, *580*, 124264. [CrossRef]
21. Nair, A.S.; Indu, J. Enhancing Noah Land Surface Model Prediction Skill over Indian Subcontinent by Assimilating SMOPS Blended Soil Moisture. *Remote. Sens.* **2016**, *8*, 976. [CrossRef]
22. Sorooshian, S.; Lawford, R.; Try, P.D.; Rossow, W.B.; Roads, J.; Polcher, J.; Sommeria, G.; Schiffer, R. Water and energy cycles: Investigating the links. *World Meteorol. Organ. Bull.* **2005**, *54*, 58–64.
23. Liang, X.; Lettenmaier, D.P.; Wood, E.F.; Burges, S.J. A simple hydrologically based model of land surface water and energy fluxes for general circulation models. *J. Geophys. Res.* **1994**, *99*, 14415–14428. [CrossRef]

24. Sellers, P.J.; Dickinson, R.E.; Randall, D.A.; Betts, A.K.; Hall, F.G.; Berry, J.A.; Collatz, G.J.; Denning, A.S.; Mooney, H.; Nobre, C.A.; et al. Modeling the Exchanges of Energy, Water, and Carbon Between Continents and the Atmosphere. *Science* **1997**, *275*, 502–509. [CrossRef]
25. Chen, F.; Mitchell, K.E.; Schaake, J.C.; Xue, Y.; Pan, H.L.; Koren, V.; Duan, Q.; Ek, M.B.; Betts, A.K. Modeling of land surface evaporation by four schemes and comparison with FIFE observations. *J. Geophys. Res.* **1996**, *101*, 7251–7268. [CrossRef]
26. Wang, X.; Xie, H.; Guan, H.; Zhou, X. Different responses of MODIS-derived NDVI to root-zone soil moisture in semi-arid and humid regions. *J. Hydrol.* **2007**, *340*, 12–24. [CrossRef]
27. Bolten, J.D.; Crow, W.T.; Zhan, X.; Jackson, T.J.; Reynolds, C. Evaluating the Utility of Remotely Sensed Soil Moisture Retrievals for Operational Agricultural Drought Monitoring. *IEEE J. Sel. Top. Appl. Earth Obs. Remote Sens.* **2010**, *3*, 57–66. [CrossRef]
28. Adegoke, J.O.; Carleton, A.M. Relations between Soil Moisture and Satellite Vegetation Indices in the U.S. Corn Belt. *J. Hydrometeorol.* **2002**, *3*, 395–405. [CrossRef]
29. Han, E.; Crow, W.T.; Holmes, T.R.; Bolten, J.D. Benchmarking a Soil Moisture Data Assimilation System for Agricultural Drought Monitoring. *J. Hydrometeorol.* **2014**, *15*, 1117–1134. [CrossRef]
30. Walker, J.P.; Houser, P.R. A methodology for initializing soil moisture in a global climate model: Assimilation of near-surface soil moisture observations. *J. Geophys. Res.* **2001**, *106*, 11761–11774. [CrossRef]
31. Mclaughlin, D. An integrated approach to hydrologic data assimilation: Interpolation, smoothing, and filtering. *Adv. Water Resour.* **2002**, *25*, 1275–1286. [CrossRef]
32. Walker, J.P.; Willgoose, G.R.; Kalma, J.D. Three-dimensional soil moisture profile retrieval by assimilation of near-surface measurements: Simplified Kalman filter covariance forecasting and field application. *Water Resour. Res.* **2002**, *38*, 37-1–37-13. [CrossRef]
33. Che, T.; Li, X.; Jin, R.; Huang, C. Assimilating passive microwave remote sensing data into a land surface model to improve the estimation of snow depth. *Remote Sens. Environ.* **2014**, *143*, 54–63. [CrossRef]
34. Brocca, L.L.; Tarpanelli, A.; Filippucci, P.; Dorigo, W.A.; Zaussinger, F.; Gruber, A.; Fernández-Prieto, D. How much water is used for irrigation? A new approach exploiting coarse resolution satellite soil moisture products. *Int. J. Appl. Earth Obs. Geoinf.* **2018**, *73*, 752–766. [CrossRef]
35. Kumar, S.V.; Peters-Lidard, C.D.; Santanello, J.A.; Reichle, R.H.; Draper, C.; Koster, R.D.; Nearing, G.S.; Jasinski, M.F. Evaluating the utility of satellite soil moisture retrievals over irrigated areas and the ability of land data assimilation methods to correct for unmodeled processes. *Hydrol. Earth Syst. Sci.* **2015**, *19*, 4463–4478. [CrossRef]
36. Lawston, P.M.; Santanello, J.A.; Franz, T.E.; Rodell, M. Assessment of Irrigation Physics in a Land Surface Modeling Framework using Non-Traditional and Human-Practice Datasets. *Hydrol. Earth Syst. Sci.* **2017**, *21*, 2953–2966. [CrossRef]
37. Blankenship, C.B.; Case, J.L.; Crosson, W.L.; Zavodsky, B.T. Correction of Forcing-Related Spatial Artifacts in a Land Surface Model by Satellite Soil Moisture Data Assimilation. *IEEE Geosci. Remote Sens. Lett.* **2018**, *15*, 498–502. [CrossRef]
38. Lievens, H.; Al Bitar, A.; Verhoest, N.E.; Cabot, F.; Lannoy, G.D.; Drusch, M.; Dumedah, G.; Franssen, H.J.; Kerr, Y.H.; Tomer, S.K.; et al. Optimization of a Radiative Transfer Forward Operator for Simulating SMOS Brightness Temperatures over the Upper Mississippi Basin. *J. Hydrometeorol.* **2015**, *16*, 1109–1134. [CrossRef]
39. Lievens, H.; Lannoy, G.D.; Al Bitar, A.; Drusch, M.; Dumedah, G.; Franssen, H.J.; Kerr, Y.H.; Tomer, S.K.; Martens, B.; Merlin, O.; et al. Assimilation of SMOS soil moisture and brightness temperature products into a land surface model. *Remote Sens. Environ.* **2016**, *180*, 292–304. [CrossRef]
40. Lannoy, G.D.; Reichle, R.H. Assimilation of SMOS brightness temperatures or soil moisture retrievals into a land surface model. *Hydrol. Earth Syst. Sci.* **2016**, *20*, 4895–4911. [CrossRef]
41. Reichle, R.H.; McLaughlin, D.; Entekhabi, D. Hydrologic Data Assimilation with the Ensemble Kalman Filter. *Mon. Weather Rev.* **2002**, *130*, 103–114. [CrossRef]
42. Dunne, S.C.; Entekhabi, D. An ensemble-based reanalysis approach to land data assimilation. *Water Resour. Res.* **2005**, *41*. [CrossRef]
43. Rodell, M.; Houser, P.R.; Jambor, U.; Gottschalck, J.; Mitchell, K.E.; Meng, C.; Arsenault, K.R.; Cosgrove, B.; Radakovich, J.D.; Bosilovich, M.G.; et al. The Global Land Data Assimilation System. *Bull. Am. Meteorol. Soc.* **2004**, *85*, 381–394. [CrossRef]
44. Kumar, S.V.; Harrison, K.W.; Peters-Lidard, C.D.; Santanello, J.A.; Kirschbaum, D.B. Assessing the Impact of L-Band Observations on Drought and Flood Risk Estimation: A Decision-Theoretic Approach in an OSSE Environment. *J. Hydrometeorol.* **2014**, *15*, 2140–2156. [CrossRef]
45. Reichle, R.H.; Koster, R.D. Global assimilation of satellite surface soil moisture retrievals into the NASA Catchment land surface model. *Geophys. Res. Lett.* **2005**, *32*. [CrossRef]
46. Zhao, L.; Yang, Z.; Hoar, T.J. Global Soil Moisture Estimation by Assimilating AMSR-E Brightness Temperatures in a Coupled CLM4-RTM-DART System. *J. Hydrometeorol.* **2016**, *17*, 2431–2454. [CrossRef]
47. Tian, X.; Xie, Z.; Dai, A.; Jia, B.; Shi, C. A microwave land data assimilation system: Scheme and preliminary evaluation over China. *J. Geophys. Res.* **2010**, *115*. [CrossRef]
48. Natali, S.M.; Schuur, E.A.; Mauritz, M.; Schade, J.D.; Celis, G.; Crummer, K.G.; Johnston, C.; Krapek, J.P.; Pegoraro, E.; Salmon, V.G.; et al. Permafrost thaw and soil moisture driving CO_2 and CH_4 release from upland tundra. *J. Geophys. Res. Biogeosci.* **2015**, *120*, 525–537. [CrossRef]

49. Zwieback, S.; Westermann, S.; Langer, M.; Boike, J.; Marsh, P.; Berg, A.A. Improving Permafrost Modeling by Assimilating Remotely Sensed Soil Moisture. *Water Resour. Res.* **2019**, *55*, 1814–1832. [CrossRef]
50. Andresen, C.G.; Lawrence, D.M.; Wilson, C.J.; McGuire, A.D.; Koven, C.D.; Schaefer, K.M.; Jafarov, E.; Peng, S.; Chen, X.; Gouttevin, I.; et al. Soil moisture and hydrology projections of the permafrost region—A model intercomparison. *Cryosphere* **2020**, *14*, 445–459. [CrossRef]
51. Streletskiy, D.A. Permafrost degradation. In *Snow and Ice-Related Hazards, Risks, and Disasters*; Academic Press: Cambridge, MA, USA, 2021.
52. Slater, A.; Lawrence, D.M. Diagnosing Present and Future Permafrost from Climate Models. *J. Clim.* **2013**, *26*, 5608–5623. [CrossRef]
53. Seo, E.; Lee, M.; Reichle, R.H. Assimilation of SMAP and ASCAT soil moisture retrievals into the JULES land surface model using the Local Ensemble Transform Kalman Filter. *Remote Sens. Environ.* **2021**, *253*, 112222. [CrossRef]
54. Albergel, C.; Rosnay, P.D.; Gruhier, C.; Muñoz-Sabater, J.; Hasenauer, S.; Isaksen, L.; Kerr, Y.H.; Wagner, W. Evaluation of remotely sensed and modelled soil moisture products using global ground-based in situ observations. *Remote Sens. Environ.* **2012**, *118*, 215–226. [CrossRef]
55. Reichle, R.H.; Crow, W.T.; Keppenne, C.L. An adaptive ensemble Kalman filter for soil moisture data assimilation. *Water Resour. Res.* **2008**, *44*. [CrossRef]
56. Al-Yaari, A.; Wigneron, J.; Dorigo, W.A.; Colliander, A.; Pellarin, T.; Hahn, S.; Mialon, A.; Richaume, P.; Fernandez-Moran, R.; Fan, L.; et al. Assessment and inter-comparison of recently developed/reprocessed microwave satellite soil moisture products using ISMN ground-based measurements. *Remote Sens. Environ.* **2019**, *224*, 289–303. [CrossRef]
57. Friedl, M.A.; Sulla-Menashe, D.; Tan, B.; Schneider, A.; Ramankutty, N.; Sibley, A.M.; Huang, X. MODIS Collection 5 global land cover: Algorithm refinements and characterization of new datasets. *Remote Sens. Environ.* **2010**, *114*, 168–182. [CrossRef]
58. Xu, L.; Abbaszadeh, P.; Moradkhani, H.; Chen, N.; Zhang, X. Continental drought monitoring using satellite soil moisture, data assimilation and an integrated drought index. *Remote Sens. Environ.* **2020**, *250*, 112028. [CrossRef]
59. Zhang, A.; Jia, G. Monitoring meteorological drought in semiarid regions using multi-sensor microwave remote sensing data. *Remote Sens. Environ.* **2013**, *134*, 12–23. [CrossRef]
60. Kichigina, N.V. Hydroclimatic changes and analysis of floods in large river basins of southern East Siberia. *Hydrol. Process.* **2013**, *27*, 2144–2152. [CrossRef]
61. Fedorova, A.; Makarieva, O.; Nesterova, N.; Shikhov, A.N.; Vinogradova, T.A. Modelling maximum discharge of the catastrophic flood at the Iya River (Irkutsk region, Russia) in 2019. In *E3S Web of Conferences*; EDP Sciences: Les Ulis, France, 2020.
62. Kalugin, A. Process-Based Modeling of the High Flow of a Semi-Mountain River under Current and Future Climatic Conditions: A Case Study of the Iya River (Eastern Siberia). *Water* **2021**, *13*, 1042. [CrossRef]
63. Mahrt, L.; Ek, M.B. The Influence of Atmospheric Stability on Potential Evaporation. *J. Appl. Meteorol. Climatol.* **1984**, *23*, 222–234. [CrossRef]
64. Ek, M.B.; Mitchell, K.E.; Lin, Y.; Rogers, E.; Grunmann, P.J.; Koren, V.; Gayno, G.A.; Tarpley, J.D. Implementation of Noah land surface model advances in the National Centers for Environmental Prediction operational mesoscale Eta model. *J. Geophys. Res.* **2003**, *108*. [CrossRef]
65. Derber, J.; Parrish, D.F.; Lord, S.J. The New Global Operational Analysis System at the National Meteorological Center. *Weather Forecast.* **1991**, *6*, 538–547. [CrossRef]
66. Liu, Y.Y.; Dorigo, W.A.; Parinussa, R.M.; Jeu, R.D.; Wagner, W.; Mccabe, M.F.; Evans, J.P.; Dijk, A.I. Trend-preserving blending of passive and active microwave soil moisture retrievals. *Remote Sens. Environ.* **2012**, *123*, 280–297. [CrossRef]
67. Dorigo, W.A.; Wagner, W.; Albergel, C.; Albrecht, F.; Balsamo, G.; Brocca, L.L.; Chung, D.; Ertl, M.; Forkel, M.; Gruber, A.; et al. ESA CCI Soil Moisture for improved Earth system understanding: State-of-the art and future directions. *Remote Sens. Environ.* **2017**, *203*, 185–215. [CrossRef]
68. Gruber, A.; Dorigo, W.A.; Crow, W.T.; Wagner, W. Triple Collocation-Based Merging of Satellite Soil Moisture Retrievals. *IEEE Trans. Geosci. Remote Sens.* **2017**, *55*, 6780–6792. [CrossRef]
69. Pradhan, A.; Nair, A.S.; Indu, J.; Kirstetter, P. Impact of sampling of GPM orbital data on streamflow simulations. *J. Hydrol.* **2021**, *593*, 125798. [CrossRef]
70. Ganesh, S.; Pradhan, A.; Indu, J. Evaluation of GPM sampling error over major basins in Indian subcontinent using bootstrap technique. *Adv. Space Res.* **2019**, *63*, 3289–3302. [CrossRef]
71. Fisher, R.A.; Koven, C.D. Perspectives on the Future of Land Surface Models and the Challenges of Representing Complex Terrestrial Systems. *J. Adv. Model. Earth Syst.* **2020**, *12*, e2018MS001453. [CrossRef]
72. Dumedah, G.; Walker, J.P. Assessment of land surface model uncertainty: A crucial step towards the identification of model weaknesses. *J. Hydrol.* **2014**, *519*, 1474–1484. [CrossRef]
73. Pradhan, A.; Indu, J. Assessment of SM2RAIN derived and IMERG based Precipitation Products for Hydrological Simulation. *J. Hydrol.* **2021**, *603*, 127191. [CrossRef]
74. Kumar, S.V.; Reichle, R.H.; Peters-Lidard, C.D.; Koster, R.D.; Zhan, X.; Crow, W.T.; Eylander, J.; Houser, P.R. A land surface data assimilation framework using the land information system: Description and applications. *Adv. Water Resour.* **2008**, *31*, 1419–1432. [CrossRef]

75. Lohmann, D.; Nolte-Holube, R.; Raschke, E. A large-scale horizontal routing model to be coupled to land surface parametrization schemes. *Tellus A* **1996**, *48*, 708–721. [CrossRef]
76. Makarieva, O.; Nesterova, N.; Fedorova, A.; Shikhovd, A.N.; Vinogradova, T. Modeling of the Summer 2019 Disastrous Floods on the Iya River (Irkutsk Oblast). *Geogr. Nat. Resour.* **2020**, *41*, 354–363. [CrossRef]